X-ray scattering

For EDXD experiments, about 0.3 ml of liquid were introduced in an amorphous quartz capillary (2 mm diameter), that was afterward sealed with a Teflon band and kept in dry atmosphere, just before the measurements.

EDXD (Energy Dispersive X-Ray Diffraction) is a variant of X-Ray diffraction that exploits the dependence of diffracted intensity on the energy of the radiation, according to the definition of the scattering variable for the Compton scattering between a photon and an electron:

$$q = \frac{4\pi sin\vartheta}{\lambda} \qquad (1)$$

This relation links the magnitude of the scattering variable (or momentum transfer) to the scattering angle (2ϑ) and to the wavelength of the incident radiation. Since the wavelength is related to the energy of the photon by the Planck equation E=hυ (h=Planck constant), we obtain

$$q = \frac{4\pi sin\vartheta}{hc}E \approx 1.014\ Esin\vartheta \qquad (2)$$

Therefore, the whole spectrum of scattered wavevectors can be obtained either by varying the angle and keeping the radiation energy fixed (Angular Dispersive, ADXD, that uses a monochromatized beam) or by using a variable-wavelength energy beam (i. e. the "white" part of the radiation emitted by an X-Ray tube – *Bremsstrahlung*) and using a single angle, or a limited number of angles (3 to 4). The scattered intensity obtained at each angle undergoes a data treatment procedure, that normalizes the measured scattered intensity for absorption and subtracts self-scattering and the inelastic Compton incoherent scattering, yielding the total coherent structure function, which is also known as "reduced intensity", I(q):

$$I(q) = I_{exp}(q) - \sum_{x=1}^{N} x_i {f_i}^2 - I_{Incoh} \qquad (3)$$

I(q) is the structural sensitive part of the recorded diffracted intensity I_{exp}, as it depends on the sum of the interference contributions of the waves scattered by the atoms of the sample, and, ultimately, on their relative distances, as the atoms, through their electrons, are the particles taking part to the scattering phenomenon (scatterers). The structure functions obtained from the different measurements (i. e. the 3-4 different angles) are finally joined to obtained a continuous spectrum in q, which in this study ranged from 0.5 to 24 $Å^{-1}$.

Several reviews on EDXD theory [1] and applications [2,3], to which the reader is referred to, were published in the past. A picture of the last prototype of EDXD instrument, with three detectors (three angles) is shown in Fig. S1.

From the Fourier Transform of I(Q), the total radial distribution function of the sample is obtained. This is a "real" space (or "direct" space) representation of the scattering, and is complementary to the I(q), as the same structural features may give a strong signature in I(Q) and a small one in the radial distribution, and *vice versa*. It is important to note that the radial distribution is a function of the (relative) distance, while the "reciprocal" space I(Q) depends on momenta, that are inversely proportional to the distance (large distance = small momentum and viceversa). The functional form chosen for the total radial distribution functions shown in this work is the "differential" one (Diff (r)), defined as:

$$D(r) - 4\pi r^2\rho_0 = Diff(r) = \frac{2r}{\pi}\int_0^{\infty} qI(q)M(q)\mathrm{r}\sin(q)dq \qquad (4)$$

In this expression, the non-structural term, due to the uniform radial distribution of particles that depends on the system density ρ, is left out. M(q) is a mathematical function used to reduce the truncation error of the Fourier Transform and to highlight the large q contributions, and is equal to $M(Q) = \frac{f^2N(0)}{f^2N(Q)}exp(-0.01Q^2)$.

The function I(Q) is related to the partial radial distribution functions descriptive of the structure and obtainable from the simulations, according to Equation (2):

$$I(q) = \sum_{i=1}^{N}\sum_{j=1}^{N} x_i x_j f_i f_j 4\pi\rho_0 \int_0^{\infty} r^2 (g_{ij}(r) - 1)\frac{sin(qr)}{qr} dr \qquad (5)$$

In the Equations (3) and (5), x_i and x_j are the numerical concentrations of the species while f_i and f_j are their Q-dependent X-ray scattering factors and ρ_0 is the bulk number density. Equation (2) is the link between experimental and model data, as the g(r)s can be calculated from molecular simulations. Comprehensive derivation of all the equations is described elsewhere.[2-4]

Considering that in this work we compare the structure functions of two different samples (di-hydrated and anhydrous, see Fig. 3 of the main text), we chose to use, for both experimental and computed patterns, the S(q) functional form, where I(q) is normalized to the concentrations of the various atomic species according to Equation 6:

$$\left(S(Q) = \frac{I(Q)}{\sum_{i=1}^{N} xifi(Q)} \right) \qquad (6)$$

This formulation allows to minimize the intensity differences due to the unlike scattering factors f_i of the atoms, thus facilitating comparison. Summarizing, the analysis of both reciprocal space (S(q)) and distance space (Diff(r)) functions is used to compare X-Ray experimental data and simulations. This methodology has been successfully applied to the study[5,6]of molecular and ionic liquids,[7, 8] as well as solutions.[9,10]

Fig. S1 – Photograph of the last prototype of EDXD diffractometer, with three detectors placed at three fixed angles

Computational Details

The simulations were carried out using AMBER16 [11] with GAFF [12] force field. Atomic charges were computed at B3LYP/6-31g(d) level of theory using Gaussian 09 and RESP algorithm. The cutoffs for Van der Waals interactions and for the real-space part of Ewald Summation was set at 10 Å. Electrostatic interactions were damped using a multiplicative dielectric constant of 1.5, equivalent to rescaling the point charges to 0.745 of their unperturbed value. This methodology has been used in a series of simulations on ionic liquids and was found to be a convenient way of considering charge polarization in an effective way[13]. All the cubic simulation boxes were prepared using PACKMOL to obtain an initial random distribution of the molecules. The initial cube edge L was set at twice the distance of the last correlation peak observed in the experimental radial distribution function (L/2), considering that Periodic Boundary Conditions (PBC) apply during the simulation, and was 25 Å in both systems. The appropriate number of molecules (choline, chloride, oxalic acid and water, at the correct molar ratio) was chosen according to experimental density. The simulations consisted of 10^7 minimization cycles, a short (500 ps) NVT phase to heat the system from 0 K to 50 K and prevent hole formation in the structure, a NPT equilibration phase (10 ns) at 300 K to equilibrate the density , a NVT equilibration phase (10 ns) at 300 K and a

NVT productive phase (2 ns) at 300 K. The timestep used was 2 fs in every step. The theoretical densities obtained after NPT phase differed from experimental value (Table2) by +1% (hydrated) and 8% (anhydrous). All the results shown are computed only on the last NVT phase. The structure factor from the simulations was obtained following our standard procedure[14].

Conductivity measurements

Conductivity measurement were carried out using a conductivity electrode (5072 from Crison, K = 10 cm^{-1}) with platinum plates constituting both the working and the counter electrodes. The electrode was coupled to an Autolab potentiostat/galvanostat Model PGSTAT12® from Metrohm. The potentiostat/galvanostat was remotely controlled by the computer using Nova 1.9 software. An electrochemical impedance scan was employed to measure the A.C. resistance of each solution, from which the relative conductivity was calculated. In the EIS experiments the amplitude of the potential perturbation was set to 50 mV. Impedance spectra were recorded within the frequency ranges 10^3–10^7Hz. During each measurement, temperature has been kept constant at each desired value by a water-bath thermostat. The temperature uncertainty is below 0.5 K.

Density measurements

Density measurements were measured at atmospheric pressure on a U-shaped vibrating tube densitometer, (DMA 5000 M, Anton Paar) fitted with a heating attachment, operating at atmospheric pressure and over a temperature range 293- 353 K. The internal calibration of the instrument was confirmed by measuring densities of air and triple-distilled water (resistivity of 18.2 MΩ cm), as recommended by the manufacturer, prior to every sample measurement. Temperature was internally controlled with Peltier units during the measurements and temperature uncertainty was around ±2 mK. The nominal repeatability of this densimeter is ±1 μg cm^{-3}; however taking into account sample handling, the repeatability was estimated nearly 500μg cm^{-3}, mainly due to the high hygroscopicity of DESs. All binary mixtures were injected at 293.15 K using non-lubricated disposable syringes (2 cm^3). Solid samples were melted and injected above their respective melting points. All syringes were charged with sample inside a dinitrogen filled AtmosBag glove bag.

Viscosity measurements

Viscosities were measured on a Bohlin (Malvern) Gemini 200 dynamic shear rheometer in parallel-plate configuration in the temperature range 293 to 353 K, which was controlled by Peltier units. A drop of sample was contained between a rotating upper plate (diameter of 40 mm,) and a fixed lower plate (60 mm in diameter). In this configuration, the shear rate is not constant with radial position, but varies from zero at the center to a maximum at the edge, with the induced shear rate being inversely proportional to the gap between the plates. For the DESs considered, the gap was 0.15 mm.

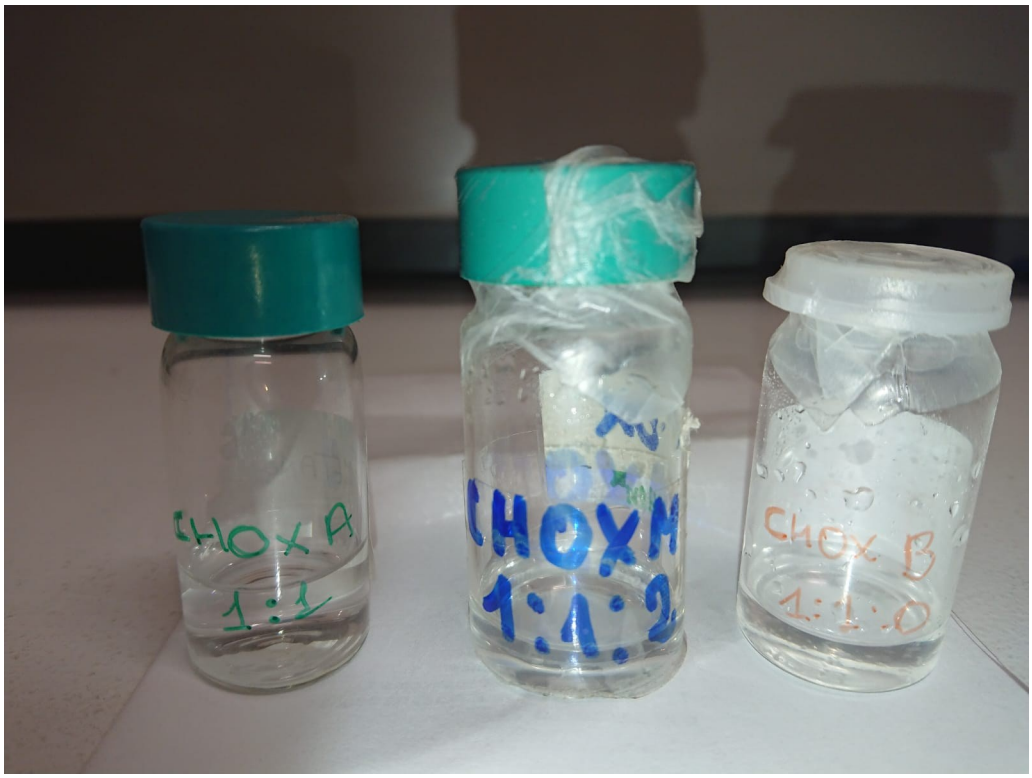

Fig. S2 – Photograph of the three liquid samples at room temperature

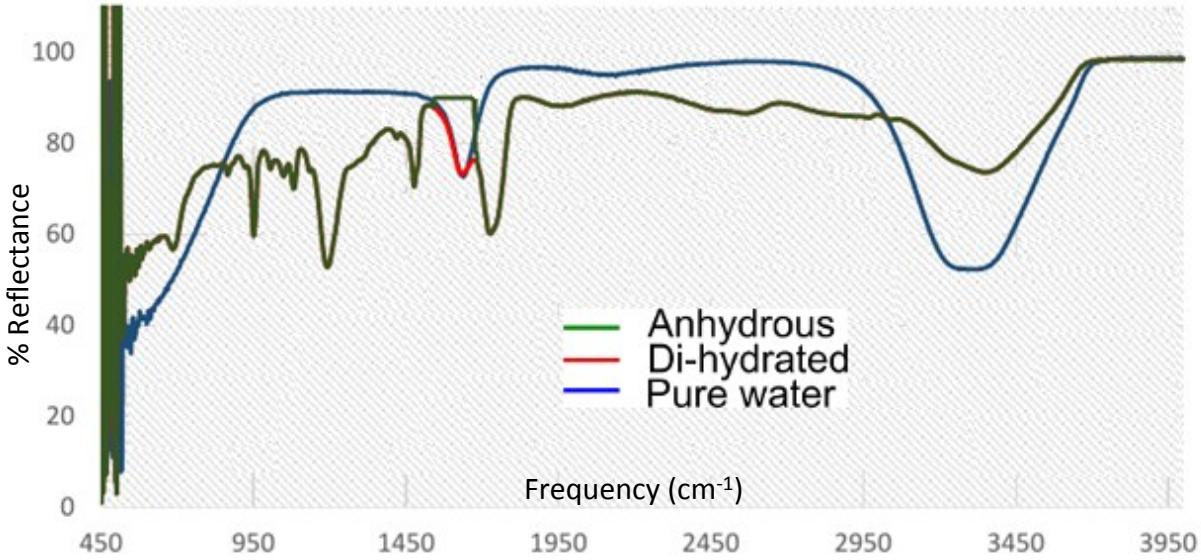

Fig. S3 –Infrared spectra (ATR) of di-hydrated (red) and anhydrous (green) compounds. Pure water (blue) is used as reference spectrum

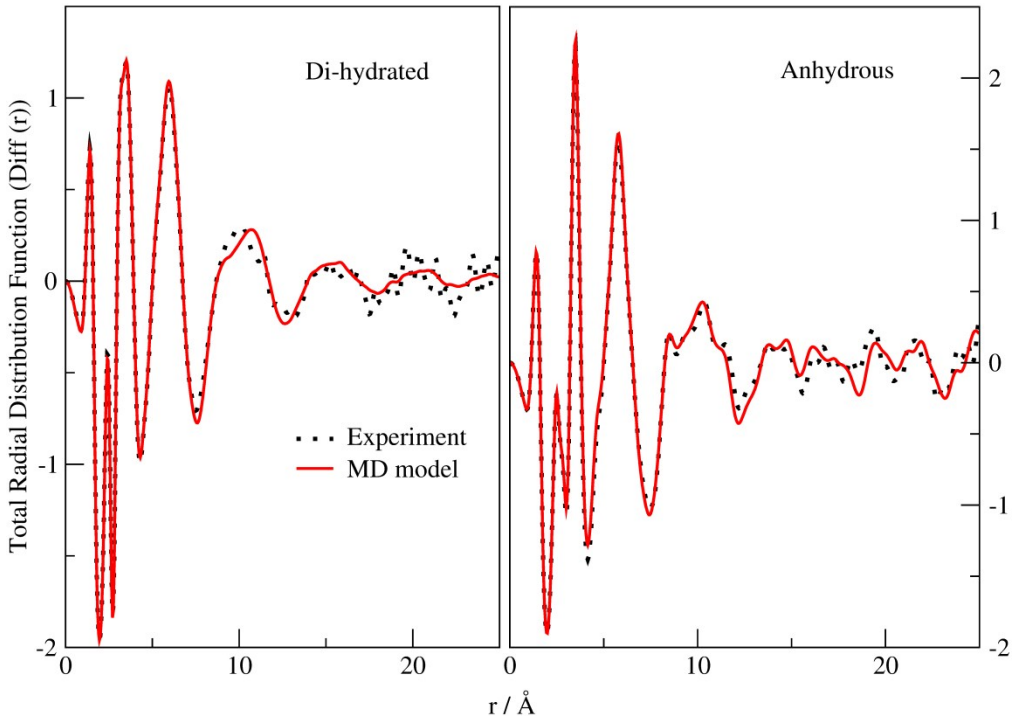

Figure S4 X-Ray Total Radial Distribution Function Diff(r) of ChClOx_M(left) and ChClOx_A (right). Dotted: experiment; continuous, red: MD model

References

(1) Rossi Albertini V, Caminiti R, The kinetics of phase transitions observed by energy-dispersive X-ray diffraction. *Int Rev PhysChem* **1999**, *18(2)*, 263-299

(2) Caminiti, R.; Carbone, M.; Mancini, G.; Sadun, C. Study of cetyltrialkylammonium bromide and tribromide salts in the solid phase. *J. Mater. Chem*. **1997**, *7*, 1331-1337

(3) Gontrani, L.; Ballirano, P.; Leonelli, F.; Caminiti, R. The structure of Ionic Liquids eds. R. Caminiti and L. Gontrani, *Springer International Publishing, Switzerland*, **2014,** 1-37

(4) Keen, D. A. A comparison of various commonly used correlation functions for describing total scattering. *J. Appl. Crystallogr***. 2001**, *34*, 172-177.

(5) Gontrani, L.; Ramondo, F.; Caracciolo, G.; Caminiti, R. A study of cyclohexane, piperidine and morpholine with X-ray diffraction and molecular simulations. *J. Mol. Liq*. **2008**, *139*, 23-28

(6) Gontrani, L.; Ramondo, F.; Caminiti, R. Energy dispersive X-ray diffraction and molecular dynamics meet: The structure of liquid pyrrole. *Chem. Phys. Lett*. **2006**, *417,* 200-205.

(7) Campetella, M.; Gontrani, L.; Bodo, E.; Ceccacci, F.; Marincola, F.; Caminiti,R. *J. Chem. Phys*. **2013**, *138 (18),* 184506

(8) Campetella, M., Gontrani, L., Bodo, E., Ceccacci, F., Cesare Marincola, F., Caminiti, R. Conformational isomerisms and nano-aggregation in substituted alkylammonium nitrates ionic liquids: An x-ray and computational study of 2-methoxyethylammonium nitrate. *J. Chem. Phys*. **2013**, *138*, 124503

(9) Mariani, A.; Dattani, R.; Caminiti, R.; Gontrani, L. Nanoscale Density Fluctuations in Ionic Liquid Binary Mixtures with Nonamphiphilic Compounds: First Experimental Evidence. *J. Phys. Chem. B*, **2016**, *120 (40)*, 10540–10546.

(10) Usula, M.; Mocci, F.; Marincola, F. C.; Porcedda, S.; Gontrani, L.; Caminiti, R. The structural organization of N-methyl-2-pyrrolidone+ water mixtures: A densitometry, x-ray diffraction, and molecular dynamics study. *J. Chem. Phys*. **2014**, *140*, 124503.

(11) Case, D.A.; Betz, R.M.; Cerutti, D.S.; Cheatham, III, T.E.; Darden, T.A.; Duke, R.E.; Giese, T.J.; Gohlke, H.; Goetz, A.W.; Homeyer, N.; Izadi, S.; Janowski, P.; Kaus, J.; Kovalenko, A.; Lee, T.S.; LeGrand, S.; Li, P.; Lin, C.; Luchko, T. ; Luo, R.; Madej, B. ; Mermelstein, D. ; Merz, K.M.; Monard, G.; Nguyen, H.; Nguyen, H.T.; Omelyan, I.; Onufriev, A.; Roe, D.R. ; Roitberg, A.; Sagui, C. ; Simmerling, C.L.; Botello-Smith, W.M.; Swails, J.; Walker, R.C.; Wang, J. ; Wolf, R.M.; Wu, X.; Xiao L. and P.A. Kollman (2016), AMBER 2016, University of California, San Francisco.

(12) Wang, J. Wolf, R. M.; Caldwell, J. W.; Kollman, P. A.; Case, D. A. Development and testing of a general amber force field*, J. Comput. Chem*. **2004**, *25*, 1157–1174; J. Wang, W. Wang, P. A. Kollman, and D. A. Case, Automatic atom type and bond type perception in molecular mechanical calculations, *J. Mol. Graphics Modell*. **2006,** *25*, 247–260

(13) Campetella, M.; Mariani, A.; Sadun, C.; Wu, B.; Castner, E. W., Jr.; Gontrani, L. Structure and dynamics of propylammonium nitrate-acetonitrile mixtures: An intricate multi-scale system probed with experimental and theoretical techniques. *J. Chem. Phys*. **2018**, *148 (13)* 134507

(14) Gontrani, L.; Ramondo, F.; Caminiti, R., Energy dispersive X-ray diffraction and molecular dynamics meet: The structure of liquid pyrrole. *Chem. Phys. Lett.* **2006**, *417 (1-3)*, 200-205.